Jurnal Kejuruteraan 35(4) 2023: 961-973
https://doi.org/10.17576/jkukm-2023-35(4)-19

The Application of OpenFOAM in Modelling Flow for Vegetated Channel

Muhammad Azizol Mohd Yusof[a]*, Suraya Sharil[a], Wan Hanna Melini Wan Mohtar[a], Azam Che Idris[b] & Anuar Mohd Yusof[c]

[a]*Department of Civil Engineering*
Faculty of Engineering & Built Environment, Universiti Kebangsaan Malaysia, Malaysia,
[b]*Universiti Brunei Darussalam, Brunei Darussalam,*
[c]*Universiti Malaysia Kelantan, Malaysia*

**Corresponding author: p111737@siswa.ukm.edu.my*

Received 5 August 2022, Received in revised form 13 February 2023
Accepted 13 March 2023, Available online 30 July 2023

ABSTRACT

Vegetation plays an important role in the hydrodynamic behaviour of an open channel flow. This study attempted to investigate the flow characteristics of an emergent vegetated channel using Open-source Operations and Manipulation (OpenFOAM). InterFoam is an OpenFOAM solver used to model this simulation. It is one of the methods available to model free-flow surface flow. Results for flow velocity profile can be generated using ParaView software. This study used a constant inlet velocity of 0.0417 m/s. There are two sets of models including model L8 with a solid volume fraction (SVF) of 8% using 9 rigid dowels, and model 4S with SVF of 4% using 17 dowels within a 1.2 m2 study area. Dowels in L8 are arranged in linear formation compared to the 4S model in a staggered arrangement. The study found that in model 4S, the stem-scale vortices are developed individually after each dowel due to sparse staggered vegetation. Meanwhile, model 8L suggests oppositely the vortex is cramped from the closeness of the dowels. The shear layer is formed as the flow enters the vegetation patch at upstream and the instability causes the shear layer vortices between inside and outside the vegetation region. Both models agreed that as the flow moves downstream the vortices are greater and make the streamwise velocity region become slower. The vertical velocity profile acknowledges the shear layer patch-scale vortices have a greater influence on the flow of both models. The magnitude of turbulence intensity in lateral directions is bigger in model 4S than in model 8L. The influence of vortices shed by upstream cylinders has an increasing impact on the irregular shedding behaviour of downstream cylinders as plant density increases. In general, the TKE values of the Model 4S are higher than those of the Model 8L. Regardless of the solid volume percentage difference, the vegetation pattern between linear and staggered has an effect on the flow. Computational Fluid Dynamic (CFD) is indeed capable to solve complex hydrodynamic characteristics.

Keywords: OpenFOAM; Emergent vegetation; Flow; Turbulence intensity; Turbulent kinetic energy

INTRODUCTION

Malaysian rivers are the major source of freshwater and contribute about 97% of the needs for the country's water resources. Vegetation is a common feature found in the downstream of rivers or any shallow aquatic system which provides several ecosystem functions such as improving the water quality, stabilising the channel bed and promotes habitat diversity. In general, vegetation is known for its capability to reduce the flow and increase deposition, as well as controlling the transport of particles through drainage or channel. Hence, it is essential for a channel, particularly a natural channel to have vegetation living along them and should be given the utmost attention by the authorities to protect and maintain the channel.

According to (Maji et al. 2020), the presence of plants in water bodies has a large effect on flow hydrodynamics, including velocity profile, turbulent kinetic energy, shear flows and drag. Certain important features such as flow rates, bed changes, and sediment carrying current capacity are influenced by aquatic plants and their hydrodynamic interactions. Parameters such as length, density, and height of vegetation may increase channel roughness and water level, subsequently decrease flow velocity. In some cases, the plants protect against riverbank erosion, tsunamis, and high waves. The experimental results show that the presence of vegetation leads to the formation of turbulence and additional drag. It is known that the distribution of vertical velocity flow depends on the density of vegetation. Increasing stem density reduces the flow velocity passing through the plants and increases velocity in areas without vegetation.

According to (Li et al. 2020) floating aquatic plants result in flow disturbances such as the flow velocity passing through the plants decreases and the flow velocity increases below the floating area. Further, changes in flow conditions will affect the transport of solute materials consisting of sediments, nutrients, contaminants, and dissolved oxygen that are in open channel ecological systems.

Aquatic vegetation also invokes changes in the flow characteristics such as turbulence structures and dissolved substance mixing processes ((Lu & Dai 2016); (Nezu & Sanjou 2008) These plants reduce sediment transport and trap pollutants ((Darby 1999); (King et al. 2012) Transportation of soluble materials is very complicated to explain in the flow of plants as plants act in controlling the flow and mixing at various scales (Kalinowska et al, 2020). Vegetation in the river contributes to the drainage and transport characteristics related to pollutants and sedimentation. Hence, understanding the flow of plants is imperative for river ecosystems and management (Yang & Choi 2010).

Laboratory experiments and computer simulations of channel flow studies have been done extensively by previous researchers. Both approaches of study have advantages and limitations which require research design in order to achieve the objective of the study. One of the main features working with computational fluid dynamics (CFD) models is the ability to fully analyse flow near the vicinity of the plant area.

CFD is a quantitative prediction method of fluid flow phenomena based on the laws of energy conservation that govern fluid movement. In CFD analysis, fluid flow inspection is based on its physical properties such as velocity, stress, temperature, density, and viscosity. The reliability of this CFD analysis depends on the entire structure of the process performed. Verification of mathematical models is important to build a suitable case for solving problems.

OpenFoam (open-source field operation and manipulation) is a licence free CFD software available on the internet. There are readily available solvers in OpenFoam for other users and solver codes are also customizable for the developer to suit specific applications. Flow structure problems can be solved by using Openfoam based on the Finite Volume Method (FVM). (Kim et al, 2020)) conducted a study on solute transport in a meandering channel using 3D RANS which is solved using Openfoam based on the FVM. Openfoam RANS model has been widely used for open channel flow analysis including study on investigation scour hole of fixed bed protection (Nguyen et al. 2018), analysis of hydraulic jump (Valles-Morán et al. 2015); (Bayon et al. 2016), turbulence model of stepped spillway, pool and weir fishway (Duguay et al. 2017) spillway jet regimes (Wang et al. 2019) and flow coupled with porous media (Kim & Kang 2020).

The purpose of this paper is to develop a model of open channel flow to explore the potential of OpenFOAM in the study of hydrodynamic parameters such as vector field, velocity distribution, turbulence intensity and turbulent kinetic energy. Studies on vegetation can be used as an attempt to solve the river management problems such as flood resistance, erosion and improving river ecological status by focusing on the characterization of hydraulic properties for vegetation that appear in open channels. At the same time, to investigate how the vegetation changes the magnitude of flow velocity and turbulence in the channel.

METHODOLOGY

METHODOLOGY FLOWCHART

The complexity of the computational flow dynamics can be softened down by planning and organising accordingly to the flow of work that must be done.

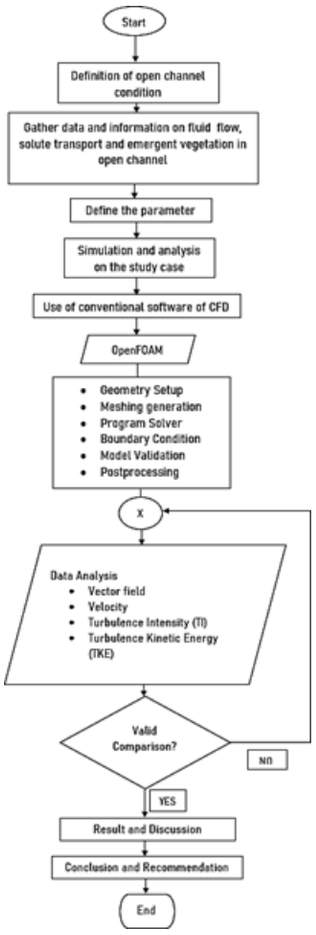

FIGURE 1. Research methodology flowchart

Figure 1 shows the research methodology flowchart which involves data gathering; model setup and simulation of OpenFOAM; data analysis and results interpretation. Research problems were studied, and necessary simplifications were made to reduce the complexity of the problem.

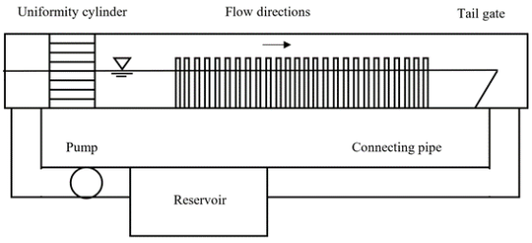

FIGURE 2. Laboratory experimental set up

Figure 2 illustrates the laboratory recirculating flume condition which at first, the water is filled up in the reservoir. A connecting pipe with pump, pumped in the water from the reservoir into the flume upstream. Before the flow enters the testing vegetation patch area, a uniformity cylinder or honeycomb hollow cylinder is placed at the inlet of water to assist the development of uniform flow. The vegetation patch is designed according to the demanded study which is emergent rigid dowels that are pre-arranged in linear and staggered configuration. The tailgate is adjusted to control the water depth of the flow. At the outlet, the flow will be channelled back into the reservoir by another connecting pipe. The water is circulated throughout the experiment.

a)

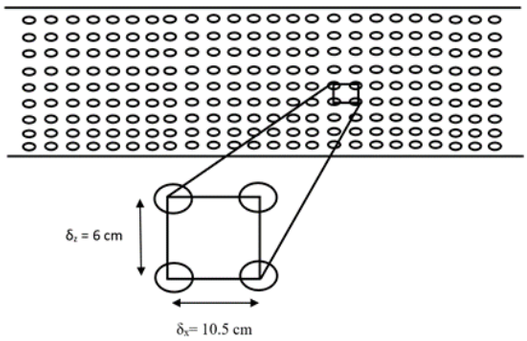

b)

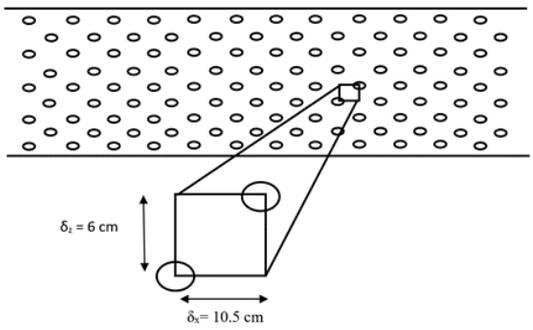

FIGURE 3. Dowels arrangement and solid volume fraction (SVF) a) Model 8L; linear and 8% density b) Model 4S; staggered and 4% density.

In Figure 3a, the dowels are arranged in linear and Figure 4b in staggered arrangement. Both models of 8L and 4S are three-dimensional with solid rod diameter of 0.025 m and the distance of between rods are arranged x = 0.105 m and z = 0.06 m. The percentage of plant density is present in solid volume fraction (SVF) of 8% and 4% respectively. SVF can be calculated with equation (1a) for linear arrangement and (1b) for staggered.

$$SVF = \frac{\pi d^2}{4\delta_x \delta_z} \quad (1a)$$

$$SVF = \frac{\pi d^2}{8\delta_x \delta_z} \quad (1b)$$

Where, d is the diameter of the dowel, δx is the distance between the centres to the centre of the dowels in the x-direction and δz is the distance between the centre to the centre of the dowels in the z-direction.

a)

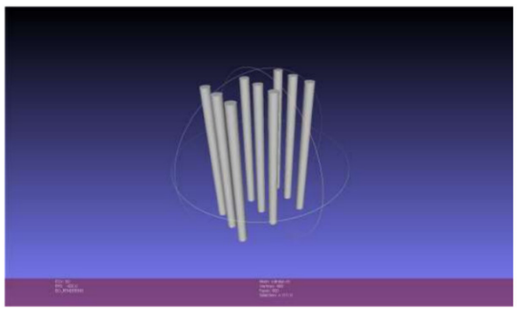

b)

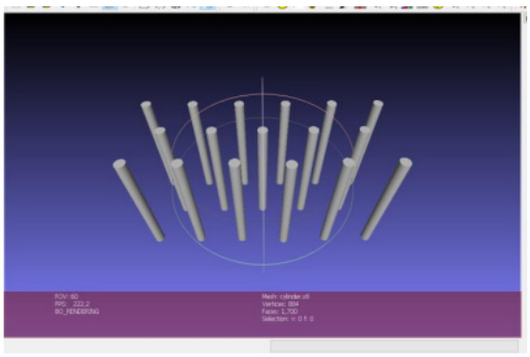

FIGURE 4. Three-dimensional dowels solid volume in FreeCAD software a) Model 8L b) Model 4S

Figure 4 presents the three-dimensional geometry of the physical model in the laboratory and computer simulation by using FreeCAD software. The software simulated nine dowels for model 8L (Figure 4a) and 17 dowels for model 4S (depicted in Figure 4b). The simplification is considered reasonable because the flow condition is uniform, and the arrangement of the dowels is repetitive.

a)

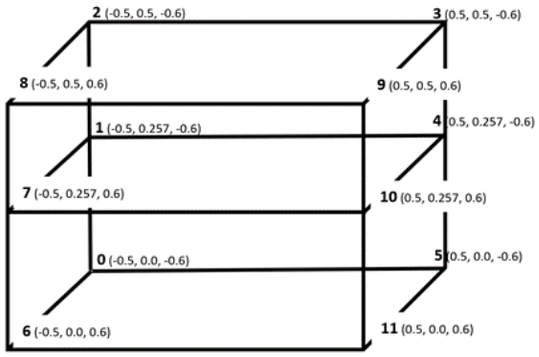

b)

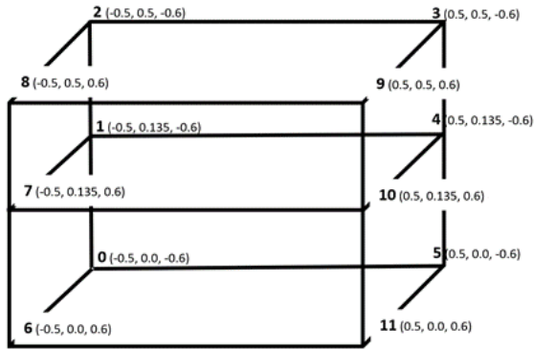

FIGURE 5. Block sampling geometry coordinates
a) Model 8L b) Model 4S

Mesh generation is the process of separating domains to subdomains. The OpenFOAM offers mesh generation for complex geometry i.e., snappyHexMesh which automatically generates a mesh according to hexahedral elements to the geometric surface. BlockMesh is one of the most basic mesh generators in OpenFOAM and it helps users build networks with blocks. To produce a mesh using blockMesh, the researcher needs to determine the vertices, the connecting blocks, and the number of cells in each direction. Researchers also need to set boundary patches to determine the connectivity of block faces. Figure 5 shows the block production for this study. The block mesh size was 1 m x 1.2 m x 0.5 m, compared to the actual flume size which was 10 m x 1.2 m and 0.5 m.

OpenFOAM SOLVER PROGRAMME

The solver used is InterFoam which has the capability for particle tracking of modelling free flow surfaces. InterFoam is a Volume of Fluid (VOF) solution for two incompressible and isothermal immiscible liquids. This means that the properties of the particles are constant in the region filled by one of the two liquids except between the phases.

PROCESSING CONDITIONS

Table 1 presented simulation conditions for model 8L and 4S. Model 8L represents 8% of SVF with linear arrangement and model 4S has 4% SVF with staggered arrangement. The same size of block mesh of 1 m x 1.2 m x 0.5 m but different flow depth of 0.257 m for model 8L and 0.135 m for model 4S.

TABLE 1. Simulation conditions

	Model	8L	4S
Vegetation properties	Solid Volume Fraction, Φ (%)	8	4
	Rod arrangement	Linear	Staggered
	Rod diameter, d (m)	0.025	
	Rod height, h (m)	0.3	
Blok mesh size	Length (m)	1.0	
	Width (m)	1.2	
	Height (m)	0.5	
	Water depth, D (m)	0.257	0.135
	Initial velocity, U_o (m)	0.0417	
	Reynold's number, Re	8248	3030

The Reynold's number is calculated using equation (2) as follows;

$$Re = \frac{U_o R}{\upsilon} \quad (2)$$

Where Uo is the initial velocity, R is the hydraulic radius and υ is the fluid kinematic viscosity. The establishment of flow conditions is foremost in this study. The flow is expressed as a laminar if Reynolds number is less than 500 and fully turbulence if greater than 12500 (Chanson et al., 1999). Thus, simulation was performed under the transitional flow regime.

SAMPLING LOCATIONS

a)

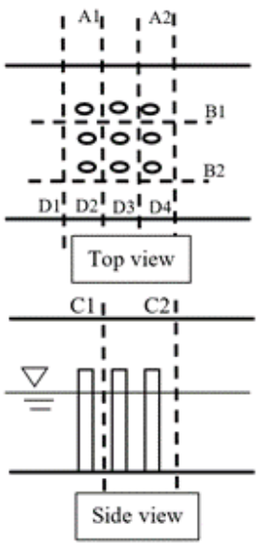

b)

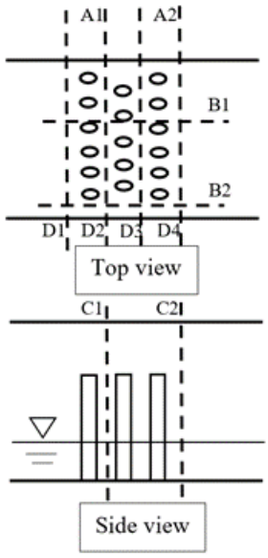

FIGURE 6. Cross-sectional sampling position lines
a) Model 8L b) Model 4S

Figure 6 shows sampling positions for model 8L and 4S are taken into account generally in the region where patch vegetation is located to observe the hydrodynamic changes. The positions are clustered as A (lateral direction), B (streamwise direction), C (vertical direction) and D (streamwise direction of turbulence intensity (TI) and turbulent kinetic energy (TKE). The numeral tagging is designate to differentiate between interior (1) and exterior (2) of patch vegetation region with exception of D, (1) observes the region before the flow enters the vegetation, (2) and (3) inside the patch region and (4) for exterior leaving the vegetation.

$$TI = \frac{U_{rms}}{\bar{U}} \quad (3a)$$

$$\bar{U} = \frac{1}{N}\sum_{i=1}^{N} u_i \quad (3b)$$

$$TKE = \frac{1}{2}(\overline{u'^2}_x + \overline{u'^2}_y + \overline{u'^2}_z) \quad (4)$$

Where, U_{rms} = root mean square velocity; U = mean velocity; u' = turbulence fluctuation; u_i = velocity.

RESULTS AND DISCUSSION

In this part, further explanation is established based on the data and observations have been through several processes of analysis. The data is tabulated or graphed according to the necessity of observation and objectives of the study.

VELOCITY PROFILES

Velocity is the premier indicator to study the behaviour of the flow through patch vegetation. The observation is made into the direction of lateral, streamwise and vertical to give better comprehension on the flow dynamics.

a)

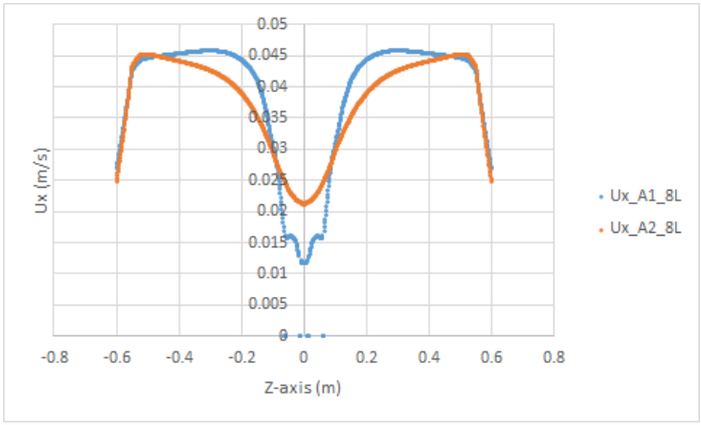

b)

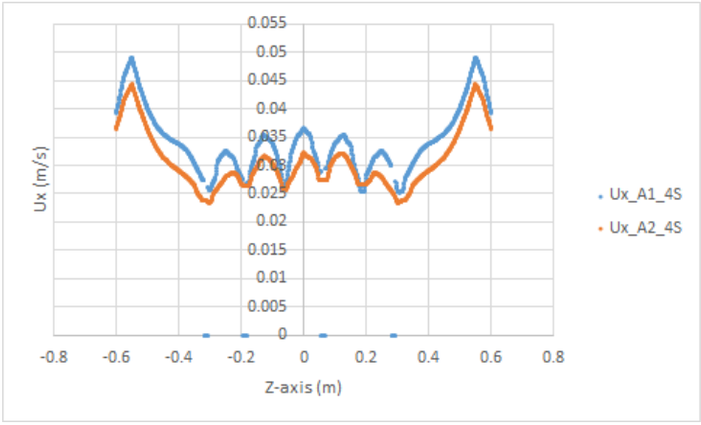

FIGURE 7. Time average velocity results from line A1 and A2 for a) Model 8L b) Model 4S

Figure 7 (a) and (b) show graphs of velocity U_x against the *Z*-axis on line A1 and A2 for model 8L and 4S. Dowels were positioned on the *Z*-axis at -0.06 m, 0 m, 0.06 m for model 8L. Dowels for model 4S were positioned at -0.3 m, -0.18 m, -0.06 m, 0.06 m, 0.18 m, 0.3 m. Line A1 presented a measurement plane within the vegetation and line A2 after the vegetation (Figure 7). Figure 7a suggested the lowest value of velocity occurred at the centreline of the patch vegetation. As the water flow travels into the vegetation region, the rods act as resistance to the flow and divert away from the curved surface of the dowel. Pressure develops just behind the dowels due to velocity gradient causing stem-scale vortices and wake generation (Nepf 2012). At the edge of the vegetation region, the velocity gradient is developed toward the free flow region due to the flow diverting away from the vegetation region. The flow is decelerated until z 0.05 m, then a shear layer is instituted causing shear layer vortices from Kelvin-Helmholtz instability (Caroppi et al. 2021). Line A2 indicates smooth s-shape distribution profiles compared to line A1 which happened to be fluctuating from z (-0.05m to 0.05m). Within the vegetation region, there are individual or multiple stem-scale vortices at the downstream of the dowel; meanwhile, leaving the edges of the vegetation region, the patch-scale vortices are noticed from the smooth s-shape transverse velocity distribution. Line A2 is also called a steady wake region until the beginning of the von Kármán vortex is developed. (Maji et al. 2020) also described the von Kármán vortex as appearing with a solid volume fraction exceeding 4%.

On the contrary, for model 4S (Figure 7b), the spatial flow velocity is showing indented distribution in the vegetation region from z (-0.3m to 0.3m). Along the *z*-axis, several parabolic velocity distributions have formed between two adjacent rod rows. The solid volume fraction of sparse vegetation condition causes the stem-scale vortices formation from each dowel and the contact vortices between two adjacent rods is prevented by the flow passing through the stem(Maji et al. 2020). The higher velocities were measured within the dowels (0.0256 to 0.036 m/s) compared to 0.023 to 0.032 m/s after the vegetation region. These results indicated the impacts of vegetation density and arrangement of the dowels (linear or staggered) towards the flow profiles. The movement of velocity particles passed through the staggered dowels is expected to be more tortuous compared to in linear arrangement. These might augment the higher velocities within dowels in comparison

to velocity profiles in linear formation (Jing et al. 2020). Nonetheless, measured velocities at A1 and A2 within and near the vegetation area were lower than the initial velocity, U_o = 0.0417 m/s.

Both models are agreeable to present that at the side of flume bank without vegetation has greater velocity values in contradictions to the vegetated region at the centre, revealing the vegetation and resistance due to it (Ahmad et al., 2020). Velocity within the dowels (A1) in model 8L simulated velocity between 0.06 to 0.045 m/s which is lower compared to 0.0158 to 0.04 m/s passing through the dowels (A2). This is more apparent in model 8L linear arrangement with dowels close to each other compared to model 4S, producing multiple effects of wakes within the vegetation region (Nepf 2004).

a)

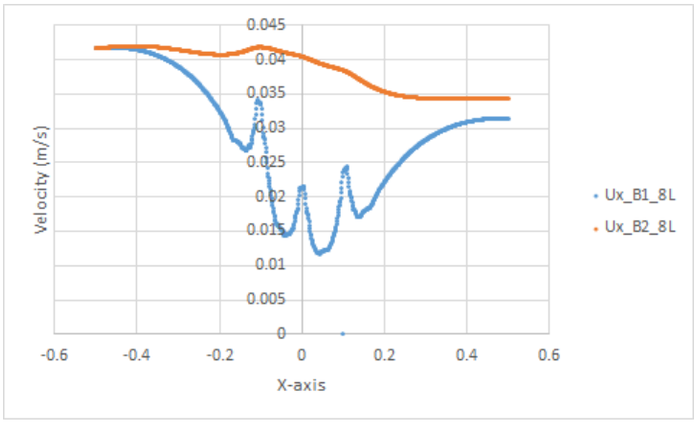

b)

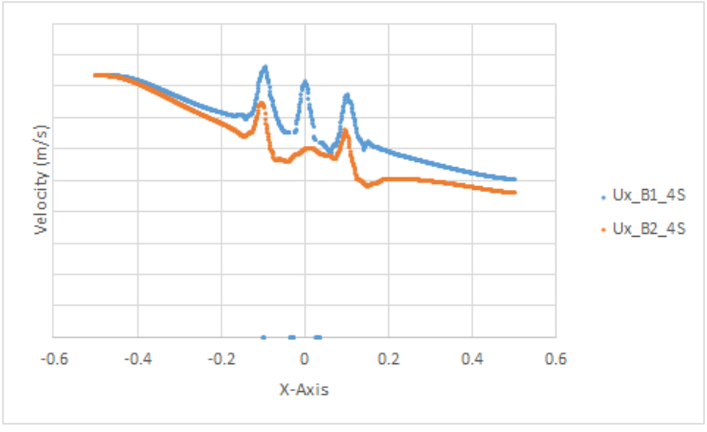

FIGURE 8. Time average velocity results from line B1 and B2 for a) Model 8L b) Model 4S

Figure 8 (a) and (b) display graphs of velocity U_x against X-axis on line B1 and B2 for model 8L and 4S. The velocity measured for model 8L (Figure 8a) at line B1 were 0.034 m/s, 0.022 m/s, and 0.024 m/s when crossing the first, the second, and the third row of the dowels. This infliction of velocity as a consequence of the detour of the flow from the dowel resulting in the creation of a shear layer. Study by (Ghani et al. 2019) also found that the infliction velocity at the frontal of dowels from the three-dimensional upward and downward of the flow resistance. The vegetation patches did not directly hinder flow, and this location was positioned adjacent to the staggered vegetation. However, after the third row, there is an infliction of velocity that is higher compared to the second column rods. This phenomenon may be due to exiting the vegetation patch, the velocity is recovering since there is no incoming vegetation to resist the flow. Line B2 was positioned outside (beside) the vegetation patch resulting in a smooth decreasing velocity profile from 0.042 to 0.038 m/s. The slightly parabolic curve velocity distribution was observed near the vegetation patch. (Ahmad et al. 2020) suggested that the presence of vegetation patches cause instability in the flow from no vegetation zone across the lateral direction from the development of coherent vortices and exchange of momentum. In general, the flow velocity of line B1 is slower compared to line B2.

The velocity profiles for model 4S (Figure 8b) show similar fluctuating patterns for B1 and B2 lines. Differ with model 8L, the velocity recorded in line B1 is slightly

higher than the velocity at line B2. Fluctuation velocity shape in Figure 8 is expected for line B1 (both model 8L and 4S) because of the dowel's position within the vegetation region. However, the velocity pattern at line B2 for model 4S, is also presenting a fluctuating pattern and lower in magnitude compared to velocity at line B1 which is opposite trend with model 8L. This possibly because of the velocity measurement position of line B2 very close to the dowels that determined the velocity profiles. (Nepf, 2004) divided velocity fields within vegetation into three regions: (1) recirculation zone downstream each dowel, (2) wake downstream the recirculation zone, (3) flow in the gaps between the wakes and dowels. Overlap wakes at region (2) may contribute to velocity deficit and flow in the gaps at region (3) potentially create a greater velocity. Nevertheless, the magnitude of flow velocities seem smaller for model 8L compared to model 4S. The SVF also plays an important role in influencing the flow velocity. Studies by (Maji et al., 2020) also found that there are strong vortexes of success in the downstream vegetation for larger SVF values. It seems like, from the lower SVF value (4%), there is a stem-scale vortex which does not significantly impact to slow down the velocity within the vegetation patch. The line B1 velocity is very much influenced by the shear layer vortices from the vegetation patch as the flow approaches the initial edge of the vegetation patch, the vortex grows downstream causing the decreasing pattern distribution.

Both models present a decrease pattern in velocity when crossing the dowels. Despite that, rod arrangement does play a role in velocity profiles where the staggered arrangement is rather causing a fluctuating pattern for both lines. In linear arrangement, parabolic patterns do occur in line B2 which represent the shear layer vortex from the Kelvin-Helmholtz (KH) instability due to patch vegetation (Nepf 2012).

a)

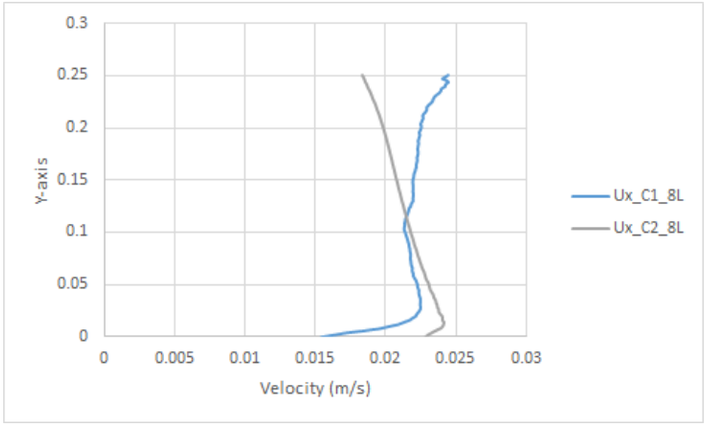

b)

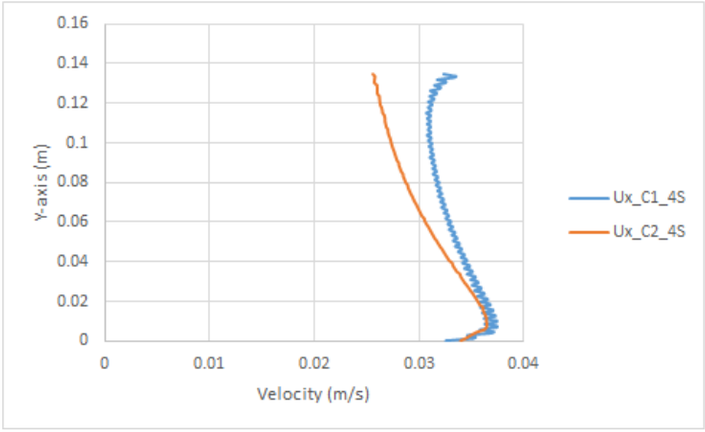

FIGURE 9. Time average velocity results from line C1 and C2 for a) Model 8L b) Model 4S

According to Figure 9a, the graph of velocity of model 8L at line C1 shows an increase in velocity along the *Y*-axis in the area of the dowels. The point of deflection occurs at 0.025 m of the *Y*-axis at which the velocity begins to decrease up to the middle of the channel and then the velocity increases from the middle of the channel to the surface of the channel for C1. The high velocity at the near free surface compared to the deflection point at the near bed shows the bed shear stress exerted on the flow is weaker than the patch vegetation (Jing et al. 2020). This situation might consider the sampling line in between the two consecutive dowels columns to cause a stem-scale shear layer. However, Line C2 recorded the deflection at 0.01m from the bed and the velocity pattern starts to decrease until the free surface. The average value of the velocity was 0.023 m/s at the bottom section, 0.021 m/s at the mid-channel, and the lowest velocity is observed at 0.018 m/s at the top free surface. This can be explained by the production of shear layer and patch-scale vortices from the Kelvin-Helmholtz instability that cause the velocity to diminish. Upstream, these vortices expand, but eventually they reach a finite width and a predetermined penetration depth into the vegetation (Nepf 2012).

Next is Figure 9b, present decreasing pattern of velocity U_x of model 4S at line C1 after the deflection point of 0.007 m and a slight increase in velocity from 0.11 m to water surface. The near bed region is heavily influenced by the bed shear stress and the bed roughness within the patch vegetation. This situation is led by the parabolic turning point of the deflection by the velocity distribution. According to (Liu et al. 2008), deflection velocity is associated with coherent structure dominated by counterclockwise vortices near the bed. As in the intermediate region to the free surface, the bed roughness does not significantly impact the velocity and in exchange with the vortex and eddies developed by the vegetation. Concurrently, line C2 shows steady decreasing of the velocity distribution starting at the deflection point at 0.007m. The lowest velocity is recorded at the near free surface region at 0.026m/s. The patch-scale transverse vortex circling in the region of vegetation edges with the free flow causes the weaker velocity which in line C2 observed (Nepf 2012).

In a general sense, model 8L vertical velocity profiles do lag behind compared to model 4S. High density of patch vegetation institutionally has been crucial as the resistance to the flow. Both models accepted the presence of patch-scale transverse vortex near the free surface region that made the velocity resisted. Nonetheless, the line C1 indicates the higher velocity at the top region will be better understood as in occupancy of patch vegetation may cause the close contact to the next cylinder then, the vortex pattern is compelled to compress. The low velocity value at the bottom shows that as the flow is within reach of the bottom, the pressure also becomes significant and creates a velocity gradient with reduced velocity (Dey et al. 2020).

Turbulence Intensity and Turbulent Kinetic Energy

Turbulence intensity (TI) and turbulent kinetic energy (TKE) are the parameters to study vortices or eddies created by the patch vegetation upon the flow. The velocity data is then to be computed to analyse both TI and TKE respectively. Table 2 shows the turbulence intensity for both models regarding x, y and z directions.

TABLE 2. Turbulence intensity (TI) in different directions and locations.

	Model 8L			Model 4S		
	TI u'(x)	TI u'(y)	TI u'(z)	TI u'(x)	TI u'(y)	TI u'(z)
D1	1.000	1.382	4.807	1.019	-1.460	-2.224
D2	1.004	1.382	7.315	1.031	-1.367	-3.916
D3	1.010	1.418	-1.036	1.045	-1.304	-9.046
D4	1.025	1.444	-1.673	1.061	-1.259	-5.783
Standard deviation	0.011	0.026	4.410	0.018	0.087	2.923

There are 4 sampling lines for transverse spatial turbulent intensity (TI) which are D1, D2, D3 and D4 taken into consideration (see Figure 6). Representing upstream is (D1) before entering the vegetation patch, within the vegetation patch (D2 and D3) and downstream (D4) leaving the vegetation patch (Table 2). The turbulent intensity values are sorted accordingly through different sampling lines at streamwise, lateral and vertical directions.

a)

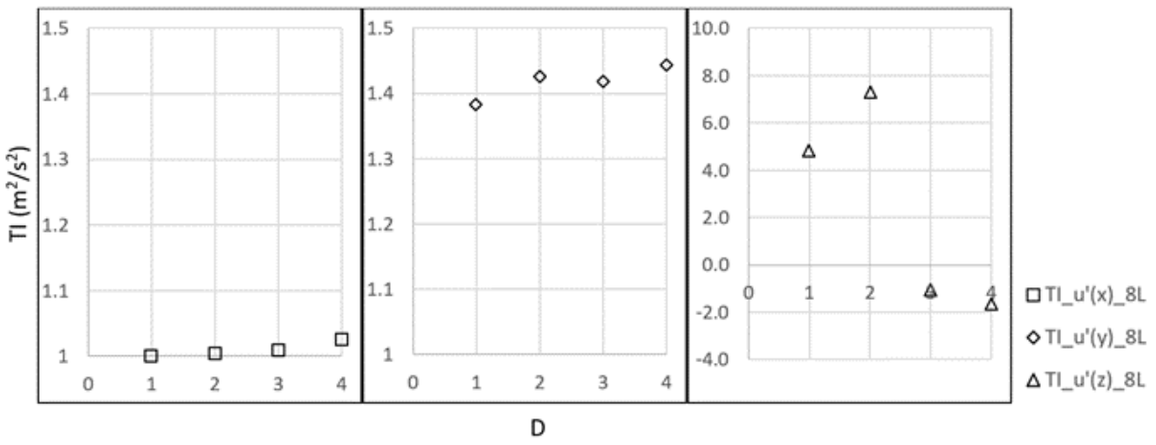

b)

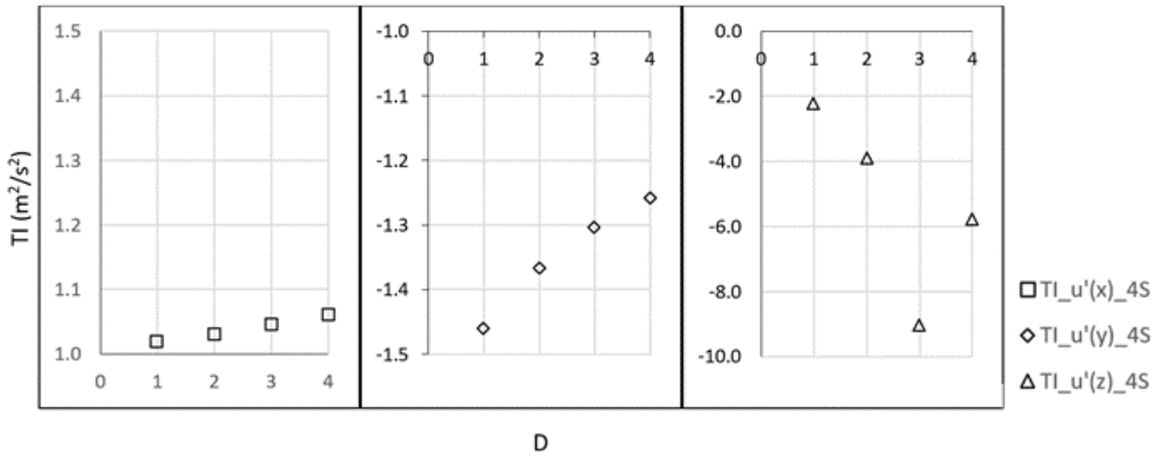

FIGURE 10. Turbulent intensity (TI) results from D1, D2,D3 and D4 for a) Model 8L b) Model 4S

Based on Figure 10, the turbulent intensity (TI) for streamwise (*x*), vertical (*y*) and lateral (*z*) were plotted against four sampling lines (D1, D2, D3 and D4). TI is calculated as the root mean square of velocities to illustrate the turbulence strength. The vegetation arrangement (linear and staggered) and vegetation density (SVF) characteristics (model 8L and Model 4S) are the main concern in choreographing the pattern of turbulent intensity at different directions. Figure 10(a) constitutes the 8L models with generally depiction *x*-direction is the lowest and *z*-direction is the greatest in experiencing turbulence. In *x*-direction, the TI is gradually increasing with the downstream (D4) being the highest although the rate of change of turbulence is small-scale. For vertical directions, the TI distribution indicates an increase pattern considering D1 is the lowest entering the vegetation patch and the value is greater leaving the vegetation patch. The dowels were positioned vertically to resist the flow and some of the flow especially in the centre of the dowel is moving in an upward direction indicating the positive value creating quasi-symmetrical turbulence. The D4 turbulent intensity is mainly affected by the patch-scale vortices that resulted in strong value. Increased vertical vorticity is accompanied by a linear rise in vorticity as the density of the plant patch increases. Furthermore, as the patch density rises, so does the frequency of vortex shedding (Stoesser et al. 2010). Since the magnitude of TI at lateral direction is the biggest, D2 sampling line location recorded the highest value followed by D1, D4 and D3. At D1, the turbulence intensity is noticed from the development of the shear layer as the patch vegetation blocks a part of the flow. Following the downstream, Kelvin-Helmholtz instability is established that enhanced shear layer vortices may contribute to strong turbulent intensity (Nepf 2012).

Figure 10(b) shows the turbulent intensity results at all directions for Model 4S. In streamwise direction, the turbulent intensity is not dense with at D4 noted greater value from the patch-scale turbulent. Meanwhile, in vertical direction, decreasing turbulent intensity distribution from entering the vegetation region until the end edge with D1 as the highest value. The momentum from the free flow when it hits the vegetation region may describe this situation (Ahmad et al. 2020). From a low SVF value with staggered

arrangement, the dowels are not close to each other, especially in a streamwise direction affecting the delays of von Karman vortex street. The highest value of turbulent intensity out of all directions happens to be the D3 sampling of lateral direction at 9 m^2/s^2. The line D3 of model 4S is situated in between the second and third row of dowels that made this region complicated and the patch-scale transverse turbulence became greater as the flow shear layer travelled downstream.

Comparing both model 8L and 4S for streamwise direction, the TI distribution pattern is almost the same with 4S model having greater value at D4. However, the turbulent intensity pattern for the 4 sampling locations of model 8L and 4S in vertical direction are completely opposite with 8L model indicated increasing and decreasing for 4S. In low SVF value, the von Karman vortex street is retarded that led the weaker reading. The magnitude of turbulent intensity in lateral directions of model 4S is more superior compared to the model 8L. (Stoesser et al. 2010) determined that vortex shedding, Kelvin-Helmholtz instability, and von Kármán-type vortices are clearly observed in sparse vegetation. The influence of vortices shed from upstream cylinders has an increasing impact on the irregular shedding behaviour of downstream cylinders as the vegetation density rises. Table 3 reveals the calculated turbulent kinetic energy (TKE) by using the equation (4).

TABLE 3. Turbulent kinetic energy (TKE)

	Model 8L	Model 4S
D1	0.00080	0.00110
D2	0.00069	0.00110
D3	0.00065	0.00100
D4	0.00068	0.00090

The tabulated data is picturize into FIGURE 11.

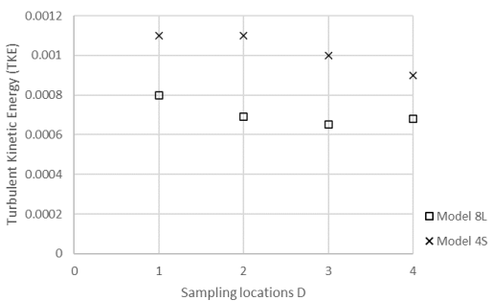

FIGURE 11. Turbulent Kinetic Energy (TKE) results from D1, D2,D3 and D4 for model 8L and model 4S

Figure 11 illustrates the Turbulent Kinetic Energy (TKE) reading from 4 sampling locations of streamwise direction. Turbulence kinetic energy (TKE) is a metric that quantifies the amount of energy produced by eddies in turbulent flow per unit mass. It may be described as root-mean-square velocity variation in the flow using the Reynolds-averaged Navier Stokes equation. Line D1 recorded highest value of TKE for both models might better be explained as the wakes, which tend to lower the flow between the bodies, dominate the mean flow, and this influence is stronger than the inviscid kinematic effect of the bodies impeding the flow. The flow is irrotational and slows upstream of the array of cylinders due to the blocking effect of the whole patch and the drag force from the cylinders. Low velocity flow bleeds through the vegetation, whereas high velocity flow bleeds through the zone devoid of vegetation (Maji et al. 2020) This phenomenon is described as the evolution of the shear layer that causes Kelvin-Helmholtz instability in the boundary layer of patch vegetation. The instability affected the creation of patch-scale vortices and a part of the vortex penetrating into the vegetation area may cause the decreasing pattern of the TKE. The energetic shear layer vortices dominate the interchange of fluxes between the open channel flow through the vegetation and the region beyond the vegetation. As the flow to the downstream, that vortex becomes weaker. Figure 11 also noted model 4S has stronger TKE values at all locations compared to model 8L. The vegetation arrangement between linear and staggered do give impact upon the flow regime. Study made by (Chang & Constantinescu 2015), the separated shear layer (SSL) was found to be longer and its eddies to have greater energy for low SVF values compared to high SVF patches. Additionally, eddies in the SSL of the low SVF patch behave in a manner similar to a mixing layer. Vortical structures were blocked, resulting in the formation of Von Kármán Street, which did not produce the typical wake vortices.

CONCLUSION

The attendance of patch vegetation does give an impact in resisting the flow. Besides that, horizontal structure such as SVF, shape and stems configuration in the emergent vegetation patch have a more critical role on the initial uniform flow and turbulence design from within to exterior of the patch in streamwise direction. In lateral direction, the velocity distribution pattern in model 8L illustrates the patch-scale vortices that cause the slower velocity at the patch vegetation. Meanwhile, for model 4S, the fluctuation velocity distribution may represent the stem-scale vortices due to sparse configuration that allow the von Karman vortex street to be fully developed. In line with the sparse configuration, model 4S has higher velocity distribution within the vegetation patch compared to model 8L.

In streamwise direction, the velocity distribution is quite different between model 8L and model 4S. However, when the flow passes the dowels, both models show a drop in velocity. Yet, rod arrangement has a role in velocity profiles, where the staggered arrangement causes a fluctuating pattern for both lines. Line B2 in the linear arrangement exhibits a parabolic pattern, with the exception of line B1, which represents the shear layer vortex from the KH instability caused by patch vegetation.

The model 8L vertical velocity profiles fall behind the model 4S. High density of patch vegetation has proven a critical flow barrier. Both models acknowledged the presence of a patch-scale transverse vortex near the free surface region, from resisted velocity. Nonetheless, the line C1 suggests a faster velocity in the top region, which will be better understood as dense vegetation occupancy may produce close contact with the next cylinder, causing the vortex pattern to compress. The low velocity number at the bottom indicates that as the flow approached the bottom, the pressure increased, generating a velocity gradient with decreasing velocity.

The TI distribution pattern is nearly the same in both models, with the 4S model having a higher value at D4. The turbulence intensity pattern for the four sample locations of models 8L and 4S in the vertical direction, on the other hand, is entirely opposite, with the 8L model indicating increasing and decreasing for 4S. Model 4S has a greater magnitude of turbulence intensity in lateral directions than model 8L. As the vegetation density increases, the influence of vortices shed by upstream cylinders has an increasing impact on the irregular shedding behaviour of downstream cylinders.

The turbulent kinetic energy (TKE) shows decreasing distribution for both models. Line D1 recorded the highest value of TKE from the flow is proportional to velocity and slows upstream of the grid of cylinders due to the patch's blocking effect and the cylinders' drag force. As the flow moves downstream, the vortex weakens. Model 4S has generally stronger TKE values in contrast with model 8L. The vegetation arrangement between linear and staggered do give impact upon the flow regardless of the solid volume fraction difference.

The Computational Fluid Dynamics (CFD) primely simulates the natural geomorphological of a natural river. OpenFOAM software has potential to study the CFD with various flow conditions, horizontal resistant, vertical resistant and different configuration of the resistance. In the future, those laboratory study results can be calibrated, and further discussion would contribute to the understanding of complex hydrodynamics.

ACKNOWLEDGEMENT

The authors acknowledge the financial support given by the Ministry of Higher Education through the Fundamental Research Grant Scheme FRGS/1/2017/TK01/UKM/03/1. Ministry of Higher Education (MOHE) and Universiti Kebangsaan Malaysia for the approved fund which makes this important research viable and effective.

DECLARATION OF COMPETING INTEREST

None

REFERENCES

Ahmad, M., Ghani, U., Anjum, N., Pasha, G. A., Ullah, M. K.. & Ahmed, A. 2020. Investigating the flow hydrodynamics in a compound channel with layered vegetated floodplains. *Civil Engineering Journal (Iran)* 6(5): 860–876. DOI: https://doi.org/10.28991/cej-2020-03091513.

Bayon, A., Valero, D., García-Bartual, R., Vallés-Morán, F. J. & López-Jiménez, P. A. 2016. Performance assessment of OpenFOAM and FLOW-3D in the numerical modeling of a low Reynolds number hydraulic jump. Environmental Modelling and Software 80: 322–335. DOI:https://doi.org/10.1016/j.envsoft.2016.02.018.

Caroppi, G., Västilä, K., Gualtieri, P., Järvelä, J., Giugni, M. & Rowiński, P. M. 2021. Comparison of Flexible and Rigid Vegetation Induced Shear Layers in Partly Vegetated Channels. Water Resources Research 57(3). DOI:https://doi.org/10.1029/2020WR028243.

Chang, K.. & Constantinescu, G. 2015. Numerical investigation of flow and turbulence structure through and around a circular array of rigid cylinders. *Journal of Fluid Mechanics* 776: 161–199. DOI:https://doi.org/10.1017/jfm.2015.321.

Chanson, H., Boston, A., London, H., Oxford, Y., San, P., San, D., Singapore, F. & Tokyo, S. 1999. The Hydraulics of Open Channel Flow: An Introduction Basic principles, sediment motion, hydraulic modelling, design of hydraulic structures Second Edition. DOI:https://doi.org/10.1016/B978-075065978-9/50026-X.

Darby, S. E. 1999. Effect of riparian vegetation on flow resistance and flood potential. In *Journal of Hydraulic Engineering*. DOI:https://doi.org/10.1061/(ASCE)0733-9429(1999)125:5(443).

Dey, S., Paul, P., Fang, H. & Padhi, E. 2020. Hydrodynamics of flow over two-dimensional dunes. *Physics of Fluids* 32(2). DOI:https://doi.org/10.1063/1.5144552.

Duguay, J. M., Lacey, R. W. J. & Gaucher, J. 2017. A case study of a pool and weir fishway modeled with OpenFOAM and FLOW-3D. *Ecological Engineering* 103: 31–42. DOI:https://doi.org/10.1016/j.ecoleng.2017.01.042.

Ghani, U., Anjum, N., Pasha, G. A. & Ahmad, M. 2019. Investigating the turbulent flow characteristics in an open channel with staggered vegetation patches. *River Research and Applications* 35(7): 966–978. DOI:https://doi.org/10.1002/rra.3460.

Jing, H. fang, Cai, Y. juan, Wang, W. hong, Guo, Y. kun, Li, C. guang & Bai, Y. chuan. 2020. Investigation of open channel flow with unsubmerged rigid vegetation by the lattice Boltzmann method. *Journal of Hydrodynamics* 32(4): 771–783. DOI:https://doi.org/10.1007/s42241-019-0072-7.

Kalinowska, M. B., Mrokowska, M. M. & Rowiński Editors, P. M. 2020. GeoPlanet: Earth and Planetary Sciences Recent Trends in Environmental Hydraulics 38th International School of Hydraulics. DOI:https://doi.org/10.1007/978-3-030-37105-0.

Kim, J. S., Baek, D. & Park, I. 2020. Evaluating the impact of turbulence closure models on solute transport simulations in meandering open channels. *Applied Sciences (Switzerland)* 10(8). DOI:https://doi.org/10.3390/APP10082769.

Kim, J. S. & Kang, P. K. 2020. Anomalous transport through free-flow-porous media interface: Pore-scale simulation and predictive modeling. *Advances in Water Resources* 135. DOI:https://doi.org/10.1016/j.advwatres.2019.103467.

King, A. T., Tinoco, R. O. & Cowen, E. A. 2012. A k-ε turbulence model based on the scales of vertical shear and stem wakes valid for emergent and submerged vegetated flows. *Journal of Fluid Mechanics* 701: 1–39. DOI:https://doi.org/10.1017/jfm.2012.113.

Li, D., Huai, W. xin & Liu, M. yang. 2020. Investigation of the flow characteristics with one-line emergent canopy patches in open channel. *Journal of Hydrology* 590. DOI:https://doi.org/10.1016/j.jhydrol.2020.125248.

Liu, D., Diplas, P., Fairbanks, J. D. & Hodges, C. C. 2008. An experimental study of flow through rigid vegetation. *Journal of Geophysical Research: Earth Surface*, 113(4). DOI:https://doi.org/10.1029/2008JF001042.

Lu, J. & Dai, H. C. 2016. Effect of submerged vegetation on solute transport in an open channel using large eddy simulation. *Advances in Water Resources* 97: 87–99. DOI:https://doi.org/10.1016/j.advwatres.2016.09.003.

Maji, S., Hanmaiahgari, P. R., Balachandar, R., Pu, J. H., Ricardo, A. M. & Ferreira, R. M. L. 2020. A review on hydrodynamics of free surface flows in emergent vegetated channels. *Water (Switzerland)* 12(4): 1–17. DOI:https://doi.org/10.3390/W12041218.

Nepf, H. M. 2004. 8 Vegetated Flow Dynamics Introduction: Scales of Morphology and Flow in a Tidal Marsh. DOI:https://doi.org/10.1029/59CE09.

Nepf, H. M. 2012. Hydrodynamics of vegetated channels. *Journal of Hydraulic Research*, 50(3): 262–279. DOI:https://doi.org/10.1080/00221686.2012.696559.

Nezu, I. & Sanjou, M. 2008. Turburence structure and coherent motion in vegetated canopy open-channel flows. *Journal of Hydro-Environment Research* 2(2): 62–90. DOI:https://doi.org/10.1016/j.jher.2008.05.003.

Nguyen, T. H. T., Lee, J., Park, S. W. & Ahn, J. 2018. Two-dimensional Numerical Analysis on the Flow and Turbulence Structures in Artificial Dunes. *KSCE Journal of Civil Engineering* 22(12): 4922–4929. DOI:https://doi.org/10.1007/s12205-018-0103-x.

Stoesser, T., Asce, M., Kim, S. J., Diplas, P. & Asce, M. 2010. Turbulent Flow through Idealized Emergent Vegetation. December, 1003–1017. DOI:https://doi.org/10.1061/(ASCE)HY.1943-7900.0000153.

Valles-Morán, F., Bayon, A. & Macián-Pérez, J. F. 2015. Hydraulic Jump Characteristic in Expanding Stilling Basin with Roughened Bed View project Experimental Investigation of Pressure Fluctuation in Spatial Hydraulic Jump View project. https://www.researchgate.net/publication/339848914

Wang, Y., Politano, M. & Weber, L. 2019. Spillway jet regime and total dissolved gas prediction with a multiphase flow model. *Journal of Hydraulic Research* 57(1): 26–38. DOI:https://doi.org/10.1080/00221686.2018.1428231.

Yang, W. & Choi, S. U. 2010. A two-layer approach for depth-limited open-channel flows with submerged vegetation. *Journal of Hydraulic Research* 48(4): 466–475. DOI:https://doi.org/10.1080/00221686.2010.491649.